Published in final edited form as:
Neurobiol Dis. 2007 January ; 25(1): 150–162.

Successive neuron loss in the thalamus and cortex in a mouse model of infantile neuronal ceroid lipofuscinosis

Catherine Kielar[1,2,3,*], **Lucy Maddox**[1,2,*], **Ellen Bible**[1,2,3], **Charlie C Pontikis**[1,2,3], **Shannon L Macauley**[4], **Megan A Griffey**[4], **Michael Wong**[5], **Mark S Sands**[4,6], and **Jonathan D Cooper**[1,2,3]

1*Pediatric Storage Disorders Laboratory, Box P040, MRC Social Genetic and Developmental Psychiatry Centre, Institute of Psychiatry, De Crespigny Park, King's College London, London, SE5 8AF, UK*

2*Department of Neuroscience, Box P040, MRC Social Genetic and Developmental Psychiatry Centre, Institute of Psychiatry, De Crespigny Park, King's College London, London, SE5 8AF, UK*

3*Centre for the Cellular Basis of Behaviour, Box P040, MRC Social Genetic and Developmental Psychiatry Centre, Institute of Psychiatry, De Crespigny Park, King's College London, London, SE5 8AF, UK*

4*Department of Internal Medicine, Washington University School of Medicine, 660 South Euclid Avenue, St. Louis, MO 63110, USA*

5*Department of Neurology, Washington University School of Medicine, 660 South Euclid Avenue, St. Louis, MO 63110, USA*

6*Department of Genetics, Washington University School of Medicine, 660 South Euclid Avenue, St. Louis, MO 63110, USA*

Abstract

Infantile neuronal ceroid lipofuscinosis (INCL) is caused by deficiency of the lysosomal enzyme, palmitoyl protein thioesterase 1 (PPT1). We have investigated the onset and progression of pathological changes in Ppt1-deficient mice (*Ppt1*$^{-/-}$) and the development of their seizure phenotype. Surprisingly, cortical atrophy and neuron loss occurred only late in disease progression, but were preceded by localized astrocytosis within individual thalamic nuclei and the progressive loss of thalamic neurons that relay different sensory modalities to the cortex. This thalamic neuron loss occurred first within the visual system and only subsequently in auditory and somatosensory relay nuclei or the inhibitory reticular thalamic nucleus. The loss of granule neurons and GABAergic interneurons followed in each corresponding cortical region, before the onset of seizure activity. These findings provide novel evidence for successive neuron loss within the thalamus and cortex in Ppt1$^{-/-}$ mice, revealing the thalamus as an important early focus of INCL pathogenesis.

Address for correspondence: Jonathan D. Cooper, Pediatric Storage Disorders Laboratory, Box P040, Department of Neuroscience and Centre for the Cellular Basis of Behaviour, MRC Social Genetic and Developmental Psychiatry Centre, Institute of Psychiatry, King's College London, De Crespigny Park, London, SE5 8AF, UK. Phone +44-20-7848-0286 ; Fax +44-20-7848-0273; E-mail : j.cooper@iop.kcl.ac.uk.

*These authors contributed equally to this study

Keywords

Infantile neuronal ceroid lipofuscinosis; Batten disease; PPT1; Thalamic neurodegeneration; Seizures, GABAergic interneurons; Lysosomal storage disorder

Introduction

Batten disease, or Neuronal Ceroid Lipofuscinosis (NCL), is the most frequent autosomal-recessive storage disorder of childhood (Cooper, 2003). At least eight forms of this fatal neurodegenerative disorder exist, each due to mutations in a different gene and characterized by the accumulation of autofluorescent storage material (Cooper, 2003; Mole et al., 2005). The different forms of NCL are typically classified by age of onset, with infantile NCL (INCL) exhibiting the earliest onset and most rapid course (Haltia et al., 1973a, 1973b; Santavuori et al., 1973). Affected children develop normally until 12 months, but subsequently undergo complete retinal degeneration and blindness, cognitive and motor deficits, seizures and a flat electroencephalogram by 3 years. These children remain in a vegetative state for several years and with no effective treatment available will invariably die (Santavuori et al., 1973; Mole et al., 2005). At autopsy these patients show massive neuronal degeneration that is most pronounced, but not confined, to the cortex (Haltia et al., 1973a, 1973b).

INCL is caused by mutations in the *CLN1* gene encoding palmitoyl protein thioesterase 1 (PPT1) a soluble lysosomal enzyme (Vesa et al., 1995), whose function is to remove long-chain fatty acids from modified cysteine residues (Hofmann et al., 2001; Lu et al., 2002). However, the precise role of PPT1 in the CNS is uncertain and the mechanisms by which PPT1 deficiency leads to the devastating clinical profile of INCL remains poorly understood. *Ppt1* null mutant mice ($Ppt1^{-/-}$) are a valuable tool for investigating these issues and display an INCL-like phenotype with marked neurodegeneration and glial responses, visual, motor and cognitive deficits and the development of spontaneous seizures (Gupta et al., 2001; Bible et al., 2004; Griffey et al., 2005, 2006).

We have previously described the pathological phenotype of severely affected $Ppt1^{-/-}$ mice, and revealed graded effects on neuron survival depending upon cellular location and phenotype (Bible et al., 2004). Recent data suggest that endoplasmic reticulum stress and activation of the unfolded protein response (Kim et al., 2006; Zhang et al., 2006), or effects upon synaptic vesicle pool size (Virmani et al., 2005), may be contributory factors leading to neuron loss in $Ppt1^{-/-}$ mice. We have now investigated the onset and progression of glial activation, thalamic and cortical neuron loss, and correlated these events in $Ppt1^{-/-}$ mice with the development of their seizure phenotype. Our data reveal an early astrocytic activation followed by selective neuronal loss and microglial responses. These events were particularly localized to the thalamus with the progressive loss of relay neurons in different thalamic nuclei and the successive death of different classes of interneurons and of granule neurons in the cortex, followed by the onset of spontaneous seizure activity. These effects upon neuron survival were more pronounced at an earlier age within the visual system, than in pathways relaying other sensory modalities. These findings provide novel data for the thalamus as a particular pathological focus in the early stages of INCL and have important implications for understanding the pathogenesis of this profoundly disabling disorder.

Materials and Methods

Ppt1-deficient mice

The *Ppt1*-deficient mice ($Ppt1^{-/-}$) used in this study were originally created through a targeted disruption strategy which eliminates the last exon in the coding sequence of *Ppt1* (Gupta et al.,

2001). These mice were subsequently backcrossed for 10 generations with C57BL/6 control mice, which is generally considered sufficient to be congenic on this strain background. C57BL/6 congenic *Ppt1*$^{-/-}$ mice and age matched C57BL/6 control mice were bred and housed in a barrier facility at Washington University School of Medicine (St. Louis, MO). All animal procedures were carried out in accordance with NIH guidelines and the Institutional Animal Care and Use Committee regulations of Washington University.

Histological analysis

Ppt1$^{-/-}$ mice present with an INCL related phenotype and usually die around 8-8.5 months of age (Gupta et al., 2001). To analyze the progression of pathological changes in the *Ppt1*$^{-/-}$ deficient CNS, the brains of *Ppt1*$^{-/-}$ mice and C57BL/6 controls were harvested at 1, 3, 5 and 7 months of age (n=3 Ppt1$^{-/-}$ and C57BL/6 control mice at each age). These brains were immersion fixed for at least one week in 4% paraformaldehyde in 0.1 M phosphate-buffered saline, cryoprotected in a solution of 30% sucrose in Tris buffered saline (TBS: 50mM Tris, pH 7.6, 150 mM NaCl) and 40μm frozen coronal sections cut through the rostrocaudal extent of the cortical mantle (Bible et al., 2004; Griffey et al., 2004, 2005). Sections were collected one per well into 96 well plates containing a cryoprotectant solution (TBS/ 30% ethylene glycol/ 15% sucrose/ 0.05% sodium azide) and stored at −40°C prior to histological processing. For quantifying autofluorescence, every sixth section from each brain was mounted on Superfrost microscope slides and coverslipped with Vectashield (Vector Laboratories, Peterborough, UK) (Griffey et al., 2004). To provide direct visualization of neuronal morphology each adjacent section was slide mounted and Nissl stained as described previously (Bible et al., 2004). All histological processing and subsequent analyses were performed with no prior knowledge of genotype or treatment group.

Quantification of Autofluorescent Storage Material

To quantify the accumulation of autofluorescent storage material during disease progression we used a previously published thresholding image analysis method to analyze confocal images collected from different CNS regions (Griffey et al., 2004). Briefly fifteen non-overlapping confocal images per section were collected from three sections through the somatosensory barrelfield cortex and thalamus, for a total of 45 images per sampling site. All images were captured using the 543 nm laser line and 40x objective on a Zeiss Pascal LSM 5 microscope (Carl Zeiss Ltd, Welwyn Garden City, UK), maintaining a consistent relative relationship between amplitude offset and detector gain between animals. Confocal images were then subjected to thresholding image analysis to determine the area of pixels in each image that contained autofluorescent material using *Image Pro Plus* image analysis software (Media Cybernetics, Chicago, IL). At each age, averages were determined for each genotype and region and then significance was determined using ANOVA with post-hoc Bonferroni.

Immunohistochemical staining

To survey the survival of cortical interneurons and to assess the degree of astrocytic and microglial activation, a one in six series of sections was immunohistochemically stained for the interneuron markers parvalbumin (PV) and somatostatin (SOM), glial fibrillary associated protein (GFAP, astrocytes) or the microglial marker F4/80 via a previously published protocol (Bible et al., 2004). These reactions used the following polyclonal primary antisera (polyclonal rabbit anti-PV, Swant, Bellinzona, Switzerland, 1:5000; rabbit anti-SOM, Peninsula Labs, Belmont, CA, USA, 1:2000; polyclonal rabbit anti-cow GFAP, DAKO, Cambridge, UK, 1:1000; monoclonal rat anti-mouse F4/80, Serotec, Oxford, UK, 1:100). Sections were then rinsed in TBS with subsequent incubation in secondary anti-serum (swine anti-rabbit [PV, SOM and GFAP], Vector Laboratories, 1:400 and mouse adsorbed rabbit anti-rat [F4/80], Vector Laboratories, 1:1000) followed by avidin-biotin-peroxidase complex (Vectastain Elite

ABC kit, Vector Laboratories). Immunoreactivity was visualised by a standard DAB reaction and sections were mounted onto slides, air dried, cleared in xylene and coverslipped with DPX (VWR, Dorset, UK).

Measurements of cortical thickness

Cortical thicknesses measurements were obtained from Nissl stained sections using *StereoInvestigator* software (Microbrightfield Inc., Williston VT), as described previously (Bible et. al., 2004; Griffey et al., 2004, 2005). These measurements from the pial surface to white matter in cortical regions that serve different functional roles including the primary motor (M1) and somatosensory barrelfield (S1BF) cortex, primary visual (V1) and primary auditory cortex (Au1) and the lateral entorhinal cortex (LEnt). As detailed previously (Bible et al., 2005; Pontikis et al., 2005), the boundaries of each cortical region were defined according to neuroanatomical landmarks described by Paxinos and Franklin (2001). In each of these cortical regions, 10 individual thickness measurements were made in each of three sections, and the mean cortical thickness of each region determined for each mouse.

Counts of neuronal number

To examine neuronal survival within individual thalamic nuclei and their target regions we used *StereoInvestigator* software to obtain unbiased optical fractionator estimates of neuronal number from PV stained (reticular thalamic nucleus and cortical interneurons), SOM stained (cortical interneurons) and Nissl stained sections (all other nuclei). These estimates were obtained for the ventral posterior nucleus (VPM/VPL), dorsal lateral geniculate nucleus (LGNd), medial geniculate nucleus (MGN), central medial (CM), reticular thalamic nucleus (Rt), PV and SOM positive interneurons and lamina IV granule neurons of S1BF and V1, with the location of each thalamic nucleus and cortical region depicted in Figure 1. These measures were performed exactly as described previously (Bible et al., 2004;Pontikis et al., 2005), with a random starting section chosen, followed by every sixth Nissl stained, PV or SOM stained section thereafter.

Quantitative analysis of glial phenotype

The optical density of GFAP and F4/80 immunoreactivity was assessed using a semi-automated thresholding image analysis, as previously described (Bible et al., 2004; Pontikis et al., 2004, 2005). Forty non-overlapping images were captured, on three consecutive sections, through the somatosensory barrelfield (S1BF) cortex and thalamus. All parameters including lamp intensity, video camera setup and calibration were maintained constant throughout image capturing. Images were subsequently analyzed using *Image Pro Plus* image analysis software (Media Cybernetics, Chicago, IL), using an appropriate threshold that selected the foreground immunoreactivity above background. This threshold was then applied as a constant to all subsequent images analyzed per batch of animals and reagent used to determine the specific area of immunoreactivity for each antigen in each region. Data were plotted graphically as the mean percentage area of immunoreactivity per field ± SEM for each region.

Assessment of seizures via electroencephalography (EEG)

C57Bl/6 controls (n=4) and Ppt1$^{-/-}$ mice at 6 (n=4), 6.5 (n=6), 7 (n=6) and 7.5 (n=7) months of age were monitored for interictal EEG activity and clinical-electrographic seizures by simultaneous video/EEG recording using chronically implanted epidural screw electrodes, as described previously (Griffey et al., 2006). At each age EEG and video data were collected during a single, continuous 48 hour monitoring session with Post-hoc analysis of seizures and interictal EEG background activity performed using *Axoscope* software (Molecular devices, Sunnyvale CA) by a board-certified clinical electro-encephalographer blinded to both genotype and treatment. Seizures were identified as discrete events with stereotypical clinical and

electrographic features, as reported previously (Griffey et al., 2006). Clinically, seizures were typically characterized by head bobbing, rearing with forelimb clonus, and occasionally generalized convulsive activity. Electrographically, the clinical manifestations were time-locked to a stereotypical EEG discharge involving a sudden tonic spike discharge which evolved in frequency and amplitude and lasted approximately 30-40 seconds (See Figure 9A). Average seizure frequency (number of seizures/48 hour period) and number of animals with seizures were calculated for each genotype and age, ***including the number of mice that did not exhibit seizures in this calculation***. Statistical analysis was performed using Kruskal-Wallis non-parametric ANOVA. For analysis of the interictal EEG background, one-minute segments obtained from every four hr of the 48 hr EEG record were randomly selected and graded with a previously described scale (Griffey et al., 2006) comprising: Grade 1 (Normal) – normal background theta rhythm with no epileptiform spikes, Grade 2 (Mildly Abnormal) – mostly normal background with some epileptiform spikes, Grade 3 (Moderately Abnormal) – mostly abnormal background with frequent epileptiform spikes, Grade 4 (Severely Abnormal) – burst-suppression pattern. A mean interictal EEG grade was calculated for each genotype and statistical comparisons were made using ANOVA with Tukey-Kramer multiple comparison post-hoc test.

Statistical analysis

The statistical significance of differences between genotypes of all quantitative data was assessed using a one-way ANOVA (SPSS 11.5 software, SPSS Inc, Chicago, IL), with statistical significance considered at $P \leq 0.05$. The mean co-efficient of error (CE) for all individual optical fractionator and Cavalieri estimates was calculated according to the method of Gundersen and Jensen (1987) and was less than 0.08 in all these analyses.

Results

Atrophy of the cortex occurs late in disease progression

Cortical atrophy is profound in INCL brains at autopsy (Haltia et al., 1973a), but this cortical thinning does not occur uniformly in Ppt1$^{-/-}$ mice and is evident to different extents in sensory vs. motor cortex (Bible et al., 2004)—To determine at which stage of disease progression these selective effects upon the cortex first become apparent, we performed thickness measurements in the primary motor cortex (M1), somatosensory barrelfield cortex (S1BF), primary visual cortex (V1), primary auditory cortex (Au1) and lateral entorhinal cortex (LEnt) of *Ppt1*$^{-/-}$ mice and age matched controls between 1 and 7 months of age. Effects upon cortical thickness in *Ppt1*$^{-/-}$ mice occurred at different rates between cortical subfields that receive information of different sensory modalities (Figure 2). The first region to be affected was V1 which was significantly thinner in *Ppt1*$^{-/-}$ mice from 5 months of age onwards (Figure 2). A similar pattern of progressive thinning was apparent in the other cortical regions of *Ppt1*$^{-/-}$ mice, but this thinning did not become significant in Au1 and M1 until 7 months of age, and did not reach significance even at 7 months of age in S1BF and LEnt (Figure 2). Taken together these data highlight that the atrophy of the cortex that is characteristic of murine INCL occurs relatively late in disease progression and reinforce that thinning of the *Ppt1*$^{-/-}$ cortex is not uniform and occurs first in the visual cortex.

Progressive accumulation of storage material in Ppt1$^{-/-}$ mice

The pathological hallmark of the NCLs is the intralysosomal accumulation of autofluorescent storage material (Cooper, 2003; Mole et al., 2005), but there is no direct evidence that this build up of lipopigments is linked to other pathological events. Focusing upon the thalamus and cortex as regions that display atrophy in *Ppt1*$^{-/-}$ mice (Bible et al., 2004), we used a thresholding image analysis method to quantify the progressive accumulation of storage material in confocal images through these regions (Griffey et al., 2004). Consistent with our

previous findings (Bible et al., 2004; Griffey et al., 2004), there was a profound accumulation of autofluorescent storage material throughout the *Ppt1*$^{-/-}$ brain, that was virtually absent from control mice of any age (Figure 3). Quantitative analysis of this autofluorescence showed a significant increase in storage material in the somatosensory barrelfield cortex and thalamus of *Ppt1*$^{-/-}$ mice at 3 months of age (Figure 3), which continued to accumulate dramatically with increasing age reaching up to 14 times the level in age-matched controls by 7 months of age. A direct comparison of the accumulation of storage material between S1BF and the thalamus revealed a remarkably similar profile of accumulation over time, suggesting that this build-up occurred at comparable rates in these two regions (Figure 3).

Localized astrocytosis occurs early in disease progression

Astrocytosis classically accompanies neuronal loss, but may also serve as an early marker of on-going neuronal damage or dysfunction (Raivich et al., 1999). Indeed, upregulation of the astrocytic marker GFAP occurs several months before overt neuronal loss in the *Cln3* null mutant mouse model of juvenile NCL (Pontikis et al., 2004) and the South Hampshire sheep model of CLN6 (Oswald et al., 2005). In order to investigate the sequence of events leading to the widespread astrocytosis seen in severely affected *Ppt1*$^{-/-}$ mice (Bible et al. 2004) we examined sections from control and mutant mice between 1 and 7 months of age stained with the astrocytic marker GFAP, and used thresholding image analysis to quantify the expression of this marker concentrating upon the cortex and thalamus.

Progressively more widespread and intense GFAP immunoreactivity was apparent with increased age in the cortex and thalamus of *Ppt1*$^{-/-}$ mice, but changed little in distribution or intensity in age-matched control mice (Figure 4A, 4C). Although appearing similar in *Ppt1*$^{-/-}$ mice and controls at 1 month of age, a marked difference in GFAP immunoreactivity was already evident between genotypes at 3 months of age. At this age intensely stained GFAP positive astrocytes were present across all laminae of M1, S1BF, and, subsequently appearing more intensely stained with increased age (Figure 4A). Initially, in Ppt1$^{-/-}$ mice at 3 months of age this GFAP immunoreactivity appeared more prominent in the deeper laminae of each cortical subfield, but with disease progression this laminar specificity became less evident. Quantitative analysis confirmed that GFAP-immunoreactivity in S1BF was indistinguishable between genotypes at 1 month of age, but was significantly increased in *Ppt1*$^{-/-}$ mice at 3 months of age and continued to increase in intensity at 5 and 7 months of age (Figure 5A).

In contrast to the cortex, astrocytosis was markedly more localized within the thalamus of *Ppt1*$^{-/-}$ mice and was confined to individual thalamic nuclei at 3 months of age, but was virtually absent from adjacent nuclei (Figure 4B). At 3 months of age GFAP immunoreactivity was present in the ventral posterior nucleus (VPM/VPL), the dorsal lateral geniculate nucleus (LGNd), the medial geniculate (MGN), mediodorsal nucleus (MD), central medial (CM) and reticular thalamic nucleus (Rt) (Figure 4B). With increased age GFAP immunoreactivity in the *Ppt1*$^{-/-}$ thalamus spread to involve successively more thalamic nuclei (Figure 4C), but nevertheless, even at 7 months of age the same thalamic nuclei which initially displayed prominent GFAP immunoreactivity exhibited more intense staining than surrounding nuclei.

Microglial activation occurs during the later stages of disease progression

Compared to astrocytosis, we have previously shown that microglial activation is considerably more localized in severely affected *Ppt1*$^{-/-}$ mice (Bible et al., 2004). The progressive and graded activation of microglia includes their transformation from ramified to brain macrophage-like morphology (Raivich et al., 1999), and may represent a sensitive marker of local neuronal damage (Streit, 2000; 2002). To determine when such microglial activation is first apparent in disease progression, we also immunohistochemically stained sections from control and mutant mice with the microglial marker F4/80. With increased age, F4/80

immunoreactivity revealed progressive microglial activation in *Ppt1*$^{-/-}$ mice compared to controls, but was comparatively delayed compared to astrocytic activation. Quantitative thresholding image analysis revealed that F4/80 immunoreactivity did not become significantly different from age matched controls until 5 months of age (Figure 5B), subsequently exhibiting a progressive increase in the expression of this marker with increased age.

Until 5 months of age staining for F4/80 was very subtle, but nonetheless revealed faintly immunoreactive microglia within the thalamus and cortex of animals of both genotypes. At 5 months of age F4/80 immunoreactivity was more prominent in the deeper laminae of the cortical mantle of *Ppt1*$^{-/-}$ mice, but with only occasional F4/80 immunoreactive microglia with brain macrophage like morphology present. In contrast, at 7 months of age microglia in *Ppt1*$^{-/-}$ mice exhibited more intense F4/80 immunoreactivity within microglia scattered within both deeper and more superficial laminae of M1, S1BF and V1 (Figure 6A), and most prominently in individual thalamic nuclei including VPM/VPL, LGNd, and MGN (Figure 6B). In these CNS regions F4/80 immunoreactive microglia displayed a range of morphologies including those with numerous ramified processes, but most prominently in microglia with brain macrophage like morphology exhibiting more swollen soma and short thickened processes (Figure 6B).

Progressive changes in thalamic neuron number precede loss of cortical neurons

Such early and spatially restricted glial responses may be indicative of an ongoing neurodegenerative process occurring within individual components of the thalamocortical system. To investigate this issue further we used unbiased stereology to document the extent of neuronal loss in Nissl stained sections within three thalamic relay nuclei that displayed prominent astrocytic activation and relay different sensory modalities to the cortex (somatosensory, ventral posterior thalamic nucleus VPM/VPL; visual, dorsal lateral geniculate nucleus LGNd; auditory, medial geniculate nucleus MGN). These thalamic sensory relay nuclei each exhibited a progressive loss of neurons in *Ppt1*$^{-/-}$ mice, but neuron loss within these nuclei first became significant at different ages and progressed at different rates (Figure 7).

Significant loss of neurons within LGNd of *Ppt1*$^{-/-}$ mice was first evident at 3 months, and was more pronounced at 5 and 7 months of age (Figure 7). In contrast, loss of MGN and VPM/VPL neurons in *Ppt1*$^{-/-}$ mice was relatively delayed and did not become significant until 5 months (Figure 7). We also investigated the survival of parvalbumin positive neurons of the reticular thalamic nucleus (Rt) which provide the major inhibitory input to the thalamus in mice and is implicated in certain forms of seizure generation (Fuentealba and Steriade, 2005). There were significantly fewer of these inhibitory Rt neurons in 7 month old Ppt1$^{-/-}$ mice, compared to either age-matched control mice or mutant mice at 5 months of age (Figure 7). We next investigated the survival of neurons within the central media1 thalamic nucleus (CM), that is also implicated in seizure generation and projects predominantly to the striatum and prelimbic cortex (Velasco et al., 2001). The CM nucleus also exhibited intense GFAP immunoreactivity in *Ppt1*$^{-/-}$ mice from 3 months of age onwards (Figure 4C), but displayed no significant loss of thalamic neurons, even in 7 month old *Ppt1*$^{-/-}$ mice (data not shown).

These changes in thalamic neuron number occurred several months before thinning of the corresponding target regions of sensory cortex (Figure 2)—To investigate the relative timing of thalamic relay neuron loss to the survival of their target neurons or interneurons within the cortex we next obtained optical fractionator estimates of neuronal number of Nissl stained lamina IV granule neurons and SOM- and PV-positive interneurons. These data were collected in both S1BF and V1, representative cortical regions whose afferent thalamic relay neurons populations degenerate at different stages of disease

progression, occurring first within visual relay neurons of LGNd (Figure 7). This analysis revealed that loss of both cortical granule and interneuron populations became significant at an earlier age within the visual system (Figure 8). A significant loss of lamina IV granule neurons was first evident in V1 at 5 months of age, but was not apparent in S1BF until 7 months of age (Figure 8). Counts of the number of GABAergic interneurons in these cortical regions revealed the same temporal pattern, being affected first in V1 and then in S1BF (Figure 8). As in other mouse models of NCL, cortical interneurons in *Ppt1*$^{-/-}$ mice displayed graded effects upon interneuron survival with SOM-positive neurons more severely affected at an earlier age than PV-positive neurons in S1BF (Figure 8). In contrast, both interneuron populations were already significantly affected by 5 months of age in V1 of *Ppt1*$^{-/-}$ mice.

Taken together these data reveal that neuronal loss within the thalamocortical system of *Ppt1*$^{-/-}$ mice is initiated within the thalamus, with neurons relaying different sensory modalities and inhibitory neurons in Rt affected at different stages of disease progression. Irrespective of the sensory modality, the loss of thalamic relay neurons always preceded the loss of interneuron populations and the subsequent loss of their corresponding target granule neurons that were only significantly affected in the later stages of disease progression.

Spontaneous seizure activity first occurs late in disease progression

The loss of neurons in the thalamic reticular nucleus or populations of GABAergic interneurons may each lead to the generation of epileptiform discharges (Fuentealba and Steriade, 2005; Magloczky and Freund, 2005). In the light of our data that these neuron populations are progressively lost in *Ppt1*$^{-/-}$ mice (Figures 7 and 8), we next explored the onset and nature of spontaneous seizure activity in these mice by EEG recordings made via chronic epidural electrodes. No seizure activity was evident until 7 months of age when 50% of the *Ppt1*$^{-/-}$ mice displayed seizures, with this number increasing to 100% of mutant mice at 7.5 months (Figure 9B). All seizures had stereotypical clinical and electrographic features (Figure 9A), as described previously (Griffey et al., 2006). Although there was no significant difference in the number of seizures per animal or the seizure duration at 7 or 7.5 months (Figure 9B), there was markedly less variation in seizure number with increased age. To investigate progressive changes in interictal EEG activity associated with these seizures we used a previously described graded scoring system (Griffey et al., 2006), to score EEG recording traces in *Ppt1*$^{-/-}$ mice. These traces revealed that *Ppt1*$^{-/-}$ mice display progressive abnormalities in the interictal EEG pattern (Figure 9B), with a significantly increased interictal EEG grade in mutant mice older than 7 months of age compared to control mice or *Ppt1*$^{-/-}$ mice at 6 or 6.5 months of age. These data reveal that the onset of background EEG abnormalities and associated seizure activity only occurs once the significant loss of thalamic and cortical neuron populations is already underway in *Ppt1*$^{-/-}$ mice.

Discussion

This study provides the first detailed description of progressive pathological changes and seizure generation in the CNS of Ppt1 deficient mice. The cortex has always been considered as the principle pathological target in INCL, but our data reveal successive waves of neuronal loss within the thalamus and its cortical target regions. This loss of thalamic relay neurons and the subsequent loss of cortical neurons were both most pronounced in the visual system. Graded effects on interneuron populations in each cortical region preceded the loss of lamina IV granule neurons and finally the development of seizures in Ppt1$^{-/-}$ mice at the end stages of disease progression. These data reveal the thalamus as an important pathological target in INCL pathogenesis and have important implications for understanding the progressive pathogenesis of this fatal pediatric disorder.

The thalamus as an early target in INCL

As in other forms of NCL, the cortex has been considered the main focus of INCL pathology with neuron loss essentially complete in the cortex and hippocampus at autopsy (Haltia et al., 1973a; Mole et al. 2005). The cortex is also severely affected in 7 month old $^{-/-}$ mice exhibiting profound atrophy and thinning of multiple subregions (Bible et al., 2004). ***In this study we provide novel evidence that these regionally selective effects and neuronal loss in the cortical mantle of Ppt1$^{-/-}$mice occur relatively late in disease progression (Figures*** 2 ***and*** 8). ***Indeed these events in the cortex are accompanied by, or in many instances appear to be preceded by, the loss of thalamic relay neurons in each sensory system*** (Figure 7). ***Nevertheless, it remains unclear whether any mechanistic link exists between these successive waves of progressive neuron loss in these interconnected brain regions.***

Our observations of profound effects upon the thalamus are consistent with data of early thalamic hypointensity in MRI studies of INCL patients (Autti et al., 1997). Identifying the molecular mechanisms that underlie the particular vulnerability of thalamic relay neurons will be of paramount importance, but lies beyond the scope of this study. Nevertheless, our data suggest that cortical neuronal loss may occur only after reduced afferent input from the thalamus. With recent data for reorganization of synapses in *Ppt1* deficient neurons (Virmani et al., 2005), it will be informative to relate such events at the synapse with neuron loss within the thalamocortical system.

Differential effects on individual thalamic nuclei in INCL have been described at autopsy (Haltia et al., 1973a), but our data now reveal that thalamic neurons relaying different sensory modalities are lost at different stages of disease progression in $^{-/-}$ mice (Figure 7). The earliest and most pronounced effects occurred within the visual system (significant loss of LGNd neurons at 3 months), followed by loss of relay neurons within auditory and somatosensory nuclei (MGN and VPM/VPL, 5 months). The relationship between electroretinogram deficits and neurodegenerative changes in the retina or optic nerve of Ppt1$^{-/-}$ mice remains unclear (Griffey et al., 2005, Lei et al., 2006), but these events accompany the period of progressive loss of visual relay neurons in LGNd in these mutant mice (Figure 7). A similar early loss of LGNd neurons is evident in Cln3 deficient mice and may underlie the visual defects characteristic of JNCL (Weimer et al., 2006). Taken together these data suggest that the primary site of pathology in multiple forms of NCL is not within the retina itself, although effects upon the optic nerve itself cannot be excluded.

The significant loss of MGN neurons in $^{-/-}$ mice is more surprising as there are no direct reports of auditory dysfunction in INCL patients. However these individuals are considered unresponsive after 3 years of age and auditory failure may contribute to this presentation. Although there are no gross or obvious abnormalities in auditory evoked brainstem responses in 7 month old $^{-/-}$ mice (Donsante A and Sands M, unpublished observations), there may be more subtle auditory deficits in $^{-/-}$ mice that are undetectable via this methodology. Nevertheless, the auditory system and other sensory relay nuclei display particularly prominent silver staining in a mouse model of late-infantile NCL (Sleat et al., 2004). Moreover, evoked somatosensory potentials are altered in patients with CLN5, INCL and JNCL (Tackmann and Kuhlendahl, 1979; Vercruyssen et al., 1982; Vanhanen et al., 1997; Lauronen et al., 1997) and it will be informative to determine if similar functional correlates can be found in *Ppt1*-deficient mice.

Progressive pathological changes in the thalamocortical system

Early and localized glial activation are apparent in Cln3 deficient mice (Pontikis et al., 2004) and in CLN6 deficient sheep (Oswald et al., 2005), many months before these animals become symptomatic. Taken together with evidence from human autopsy material, it is apparent that

neuron-glia interactions are remarkably localized in multiple forms of NCL (Tyynelä et al., 2004), unlike the widespread accumulation of autofluorescent storage material that characterizes these disorders. Our present findings extend these observations and reveal the early activation of astrocytes within individual thalamic nuclei, followed by neuronal loss and microglial activation (Figures 4-7). Several lines of evidence suggest that astrocytes are not merely reactive, but instead play a more dynamic role influencing brain function, especially at the synapse (Perea and Araque, 2005 and 2006; Allen and Barres 2005). As such, the localized and early activation of astrocytes within thalamic nuclei that subsequently exhibit neuron loss highlight the importance of neuron-astrocyte interactions in the early stages of INCL pathogenesis. It will be important to determine whether these early astrocytic responses in *Ppt1*$^{-/-}$ mice are protective in nature, as has been suggested by the encircling of persisting neurons by GFAP positive processes in human NCL autopsy material (Tyynelä et al., 2004), a feature that is not apparent in other lysosomal disorders.

Microglial activation is generally considered a sensitive indicator of ongoing neuron dysfunction (Raivich et al., 1999; Streit 2000, 2002). The distribution of microglial activation within the thalamus in *Ppt1*$^{-/-}$ mice was very similar to that of astrocytosis, but accompanied significant neuronal loss, becoming more pronounced in the later stages of disease progression. However, a first wave of localized microglial activation also occurs before birth in CLN6 deficient sheep (Kay et al., 2006), before declining in the early postnatal period (Oswald et al., 2005). The significance of such early microglial responses in NCL pathogenesis remains unclear, but the distribution of this early microglial activation accurately predicts where neuronal loss subsequently occurs (Oswald et al., 2005).

Thalamocortical neuron loss and clinical presentation of INCL

Deterioration of vision is typically the first clinical manifestation in children with multiple forms of NCL (Santavuori et al., 1973; Mole et al., 2005). Consistent with data from a mouse model of JNCL (Weimer et al., 2006), our present data reveal that visual relay neurons in *Ppt1*$^{-/-}$ mice are affected before neurons relaying other sensory modalities. Another major clinical sign in children with INCL is the development of progressively worsening seizure activity (Santavuori et al., 1973; Mole et al., 2005), which we have now detailed for the first time in *Ppt1*$^{-/-}$ mice. Although the precise cellular basis for these seizures is not yet known, our present data suggest several candidate mechanisms of epileptogenesis including the death or dysfunction of different neuron subpopulations. The onset of spontaneous seizures in *Ppt1*$^{-/-}$ mice only occurs after the loss of populations of cortical interneurons, which are also affected in multiple forms of NCL (Cooper et al., 1999; Oswald et al., 2004; Bible et al., 2004; Pontikis et al., 2004; Tyynelä et al., 2004). Such a loss of inhibitory interneurons is frequently hypothesized as a central mechanism of epileptogenesis in human epilepsy (Magloczky and Freund, 2005) and is likely to have a significant impact upon cortical excitability in *Ppt1*$^{-/-}$ mice. It is also possible that the earlier loss of neurons in the thalamus may also contribute to seizure generation, with a significant loss of neurons in the reticular thalamic nucleus which is implicated in some forms of seizure activity (Fuentealba and Steriade, 2004). Indeed, given the inhibitory influence of the reticular nucleus upon thalamocortical projections, the selective loss of these neurons may have more significant implications for cortical activity in *Ppt1*$^{-/-}$ mice (Fuentealba and Steriade, 2004). In addition to the effects of neuronal death, the dysfunction of surviving neurons due to a loss of Ppt1 activity could also contribute to neuronal hyperexcitability and seizures. Furthermore, instead of being caused solely by neuronal abnormalities, epileptic discharges may also have a non-neuronal origin as there is considerable evidence for the modulatory influence of astrocytes upon neuronal excitability (Voltera and Meldolesi, 2005). Indeed, recent studies indicate that astrocyte dysfunction may play a central role in seizure generation (Tian et al., 2005). Although,

the early and progressive astrocytosis in *Ppt1*$^{-/-}$ mice may promote seizures, it will be important to address the specific mechanisms of epileptogenesis in these mice more directly.

Our data have provided novel evidence for a pathological cascade that is initiated within the thalamus, only subsequently impacting the cerebral cortex. These pathological changes are mirrored by the progressive development of visual defects (Griffey et al., 2005) and delayed advent of seizure activity (this study). Data of this type are particularly important for understanding pathogenesis and linking pathology to functional and behavioral changes. These data will also be essential for optimizing and fine-tuning therapeutic approaches for INCL. Indeed, placing additional injections of virus directly into the thalamus, before the damage in this brain region becomes irreversible, may provide a means to improve the therapeutic efficacy of gene transfer experiments in *Ppt1* deficient mice (Griffey et al., 2004, 2006).

Acknowledgements

These studies were supported by National Institutes of Health grants NS41930 (JDC), NS043205 (MSS), European Commission 6th Framework Research Grant LSHM-CT-2003-503051 (JDC). The following non-profit agencies also contributed financially to this work: The Batten Disease Support and Research Association (MSS, JDC, CK, EB), The Natalie Fund (JDC), The Batten Disease Family Association (JDC) and the Remy Fund (JDC). We would like to thank the other members of the PSDL for their valuable contributions; Noreen Alexander for her expert advice; Drs. David Pearce, Jaana Tyynelä, Tomas Gillingwater, Gerald Finnerty and Alison Barnwell for constructive comments on the manuscript.

References

Allen NJ, Barres BA. Signaling between glia and neurons: focus on synaptic plasticity. Curr.Opin.Neurobiol 2005;15:542–548. [PubMed: 16144764]

Autti T, Raininko R, Santavuori P, Vanhanen SL, Poutanen VP, Haltia M. MRI of neuronal ceroid lipofuscinosis. II. Postmortem MRI and histopathological study of the brain in 16 cases of neuronal ceroid lipofuscinosis of juvenile or late infantile type. Neuroradiology 1997;39:371–377. [PubMed: 9189886]

Bible E, Gupta P, Hofmann SL, Cooper JD. Regional and cellular neuropathology in the palmitoyl protein thioesterase-1 (PPT1) null mutant mouse model of infantile neuronal ceroid lipofuscinosis. Neurobiol. Dis 2004;16:346–359. [PubMed: 15193291]

Cooper JD, Messer A, Feng AK, Chua-Couzens J, Mobley WC. Apparent loss and hypertrophy of interneurons in a mouse model of neuronal ceroid lipofuscinosis: evidence for partial response to insulin-like growth factor-1 treatment. J Neurosci 1999;19:2556–2567. [PubMed: 10087069]

Cooper JD. Progress towards understanding the neurobiology of Batten disease or neuronal ceroid lipofuscinosis. Curr. Opin. Neurol 2003;16:121–128. [PubMed: 12644737]

Fuentealba P, Steriade M. The reticular nucleus revisited: intrinsic and network properties of a thalamic pacemaker. Prog Neurobiol 2005;75:125–141. [PubMed: 15784303]

Griffey M, Bible C, Vogler C, Levy B, Gupta P, Cooper JD, Sands MS. Adeno-associated virus 2 - mediated gene therapy decreases autofluorescent storage material and increases brain mass in a murine model of Infantile Neuronal Ceroid Lipofuscinosis (INCL). Neurobiol. Dis 2004;16:360–369. [PubMed: 15193292]

Griffey M, Macauley SL, Ogilvie JM, Sands MS. AAV2-Mediated Ocular Gene Therapy for Infantile Neuronal Ceroid Lipofuscinosis. Mol Ther 2005;12:413–421. [PubMed: 15979943]

Griffey MA, Wozniak D, Wong M, Bible E, Johnson K, Rothman MR, Wentz AE, Cooper JD, Sands MS. CNS-directed AAV2-mediated gene therapy ameliorates functional deficits in a murine model of infantile neuronal ceroid lipofuscinosis. Mol Ther 2006;13:538–547. [PubMed: 16364693]

Gundersen HJ, Jensen EB. The efficiency of systematic sampling in stereology and its prediction. J. Microsc 1987;147:229–263. [PubMed: 3430576]

Gupta P, Soyombo AA, Atashband A, Wisniewski KE, Shelton JM, Richardson JA, Hammer RE, Hofmann SL. Disruption of PPT1 or PPT2 causes neuronal ceroid lipofuscinosis in knockout mice. Proc. Natl. Acad. Sci. USA 2001;98:13566–13571. [PubMed: 11717424]

Haltia M, Rapola J, Santavuori P. Infantile type of so-called neuronal ceroidlipofuscinosis. Histological and electron microscopic studies. Acta Neuropathol. (Berl) 1973a;26:157–170. [PubMed: 4763201]

Haltia M, Rapola J, Santavuori P, Keranen A. Infantile type of so-called neuronal ceroid-lipofuscinosis. 2. Morphological and biochemical studies. J. Neurol. Sci 1973b;18:269–285. [PubMed: 4121459]

Hofmann SL, Das AK, Lu JY, Soyombo AA. Positional candidate gene cloning of CLN1. Adv Genet 2001;45:69–92. [PubMed: 11332777]

Kay GW, Palmer DN, Rezaie P, Cooper JD. Prenatal activation of non-neuronal cells within the developing CNS of sheep with neuronal ceroid lipofuscinosis (CLN6). Brain Pathol. 2006(In press)

Kim SJ, Zhang Z, Hitomi E, Lee YC, Mukherjee AB. Endoplasmic reticulum stress-induced caspase-4 activation mediates apoptosis and neurodegeneration in INCL. Hum Mol Genet 2006;15:1826–1834. [PubMed: 16644870]

Lauronen L, Heikkila E, Autti T, Sainio K, Huttunen J, Aronen HJ, Korvenoja A, Ilmoniemi RJ, Santavuori P. Somatosensory evoked magnetic fields from primary sensorimotor cortex in juvenile neuronal ceroid lipofuscinosis. J Child Neurol 1997;12:355–360. [PubMed: 9309517]

Lei B, Tullis GE, Kirk MD, Zhang K, Katz ML. Ocular phenotype in a mouse gene knockout model for infantile neuronal ceroid lipofuscinosis. J Neurosci Res. 2006[Epub ahead of print]

Lu Y, Verkruyse LA, Hofmann SL. The effects of lysosomotropic agents on normal and INCL cells provide further evidence for the lysosomal nature of palmitoyl-protein thioesterase function. Biochim. Biophys. Acta 2002;1583:35–44. [PubMed: 12069847]

Magloczky Z, Freund TF. Impaired and repaired inhibitory circuits in the epileptic human hippocampus. Trends Neurosci 2005;28:334–340. [PubMed: 15927690]

Mole SE, Williams RE, Goebel HH. Correlations between genotype, ultrastructural morphology and clinical phenotype in the neuronal ceroid lipofuscinoses. Neurogenetics 2005;6:107–126. [PubMed: 15965709]

Oswald MJ, Palmer DN, Kay GW, Shemilt SJA, Rezaie P, Cooper JD. Glial activation spreads from specific cerebral foci and precedes neurodegeneration in presymptomatic ovine neuronal ceroid lipofuscinosis (CLN6). Neurobiol. Dis 2005;20:49–63. [PubMed: 16137566]

Paxinos, G.; Franklin, KBJ. The mouse brain in stereotaxic coordinates. Second Edition. Academic Press; San Diego: 2001.

Perea G, Araque A. Glial calcium signaling and neuron-glia communication. Cell Calcium 2005;38:375–382. [PubMed: 16105683]

Perea G, Araque A. Synaptic information processing by astrocytes. J.Physiol. Paris. J Physiol Paris 2006;99:92–97.

Pontikis CC, Cella CV, Parihar N, Lim MJ, Chakrabarti S, Mitchison HM, Mobley WC, Rezaie P, Pearce DA, Cooper JD. Late onset neurodegeneration in the *Cln3*$^{-/-}$ mouse model of juvenile neuronal ceroid lipofuscinosis is preceded by low level glial activation. Brain Res 2004;1023:231–242. [PubMed: 15374749]

Pontikis CC, Cotman SL, MacDonald ME, Cooper JD. Thalamocortical neuron loss and localized astrocytosis in the *Cln3*$^{\Delta ex7/8}$ knock-in mouse model of Batten disease. Neurobiol. Dis 2005;20:823–836. [PubMed: 16006136]

Raivich G, Bohatschek M, Kloss CU, Werner A, Jones LL, Kreutzberg GW. Neuroglial activation repertoire in the injured brain: graded response, molecular mechanisms and cues to physiological function. Brain Res 1999;30:77–105.

Santavuori P, Haltia M, Rapola J, Raitta C. Infantile type of so-called neuronal ceroid lipofuscinosis 1: a clinical study of 15 patients. J.Neurol.Sci 1973;18:257–267. [PubMed: 4698309]

Sleat DE, Wiseman JA, El-Banna M, Kim KH, Mao Q, Price S, Macauley SL, Sidman RL, Shen MM, Zhao Q, Passini MA, Davidson BL, Stewart GR, Lobel P. A mouse model of classical late-infantile neuronal ceroid lipofuscinosis based on targeted disruption of the CLN2 gene results in a loss of tripeptidyl-peptidase I activity and progressive neurodegeneration. J Neurosci 2004;24:9117–9126. [PubMed: 15483130]

Streit WJ. Microglial response to brain injury: a brief synopsis. Toxicol Pathol 2000;28:28–30. [PubMed: 10668987]

Streit WJ. Microglia as neuroprotective, immunocompetent cells of the CNS. Glia 2002;40:133–139. [PubMed: 12379901]

Tian GF, Azmi H, Takano T, Xu Q, Peng W, Lin J, Oberheim N, Lou N, Wang X, Zielke HR, Kang J, Nedergaard M. An astrocytic basis for epilepsy. Nat Med 2005;11:973–981. [PubMed: 16116433]

Tackmann W, Kuhlendahl D. Evoked potentials in neuronal ceroid lipofuscinosis. Eur. Neurol 1979;18:234–242. [PubMed: 488141]

Tyynelä J, Cooper JD, Khan MN, Shemilt SJA, Haltia M. Hippocampal pathology in the human neuronal ceroid-lipofuscinoses: distinct patterns of storage deposition, neurodegeneration and glial activation. Brain Pathol 2004;14:349–357. [PubMed: 15605981]

Vanhanen SL, Sainio K, Lappi M, Santavuori P. EEG and evoked potentials in infantile neuronal ceroid-lipofuscinosis. Dev. Med.Child Neurol 1997;39:456–463. [PubMed: 9285436]

Velasco M, Velasco F, Velasco AL. Centromedian-thalamic and hippocampal electrical stimulation for the control of intractable epileptic seizures. J Clin Neurophysiol 2001;18:495–513. [PubMed: 11779964]

Vercruyssen A, Martin JJ, Ceuterick C, Jacobs K, Swerts L. Adult ceroid-lipofuscinosis: diagnostic value of biopsies and of neurophysiological investigations. J. Neurol., Neurosurg. Psychiatry 1982;45:1056–1059. [PubMed: 6294251]

Vesa J, Hellsten E, Verkruyse LA, Camp LA, Rapola J, Santavuori P, Hofmann SL, Peltonen L. Mutations in the palmitoyl protein thioesterase gene causing infantile neuronal ceroid lipofuscinosis. Nature 1995;376:584–587. [PubMed: 7637805]

Virmani T, Gupta P, Liu X, Kavalali ET, Hofmann SL. Progressively reduced synaptic vesicle pool size in cultured neurons derived from neuronal ceroid lipofuscinosis-1 knockout mice. Neurobiol. Dis 2005;20:314–323. [PubMed: 16242638]

Voltera A, Meldolesi J. Astrocytes, from brain glue to communication elements: the revolution continues. Nature Neuroscience Reviews 2005;6:626–640.

Weimer JM, Custer AW, Benedict JW, Alexander NA, Kingsley E, Federoff HJ, Cooper JD, Pearce DA. Visual deficits in a mouse model of Batten disease are the result of optic nerve degeneration and loss of dorsal lateral geniculate thalamic neurons. Neurobiol. Dis 2006;22:284–293. [PubMed: 16412658]

Zhang Z, Lee YC, Kim SJ, Choi MS, Tsai PC, Xu Y, Xiao YJ, Zhang P, Heffer A, Mukherjee AB. Palmitoyl-protein thioesterase-1 deficiency mediates the activation of the unfolded protein response and neuronal apoptosis in INCL. Human Molecular Genetics 2006;15:337–346. [PubMed: 16368712]

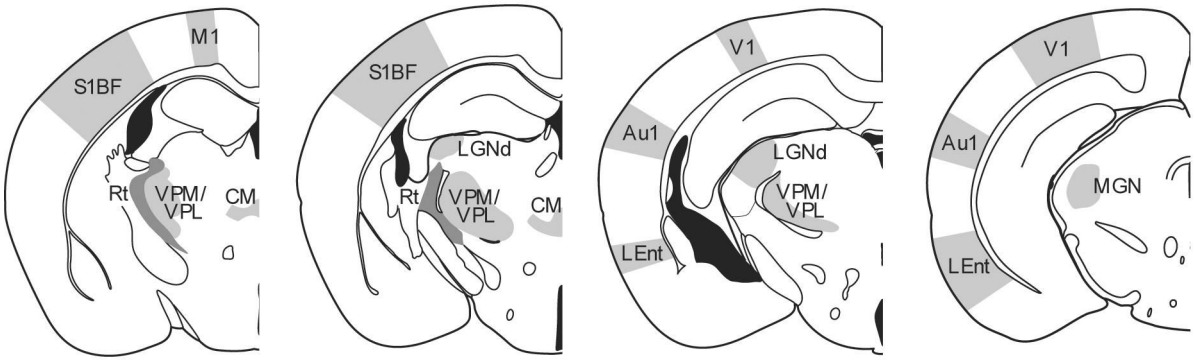

Figure 1.

Schematic diagram of the thalamic nuclei and cortical regions analyzed in *Ppt1*$^{-/-}$ mice. Measurements of cortical thickness were made in primary motor (M1) and somatosensory barrelfield (S1BF) cortex, primary visual (V1) and primary auditory cortex (Au1) and the lateral entorhinal cortex (***LEnt***), together with optical fractionator estimates of the number of lamina IV granule neurons and parvalbumin or somatostatin positive interneurons in S1BF and V1. The same unbiased stereological method was used to investigate the survival of thalamic relay neurons in the ventral posterior nucleus (VPM/VPL), dorsal lateral geniculate nucleus (LGNd), medial geniculate nucleus (MGN), central medial (CM), and of parvalbumin positive inhibitory neurons in the reticular thalamic nucleus (Rt, darker shading) at different stages of disease progression.

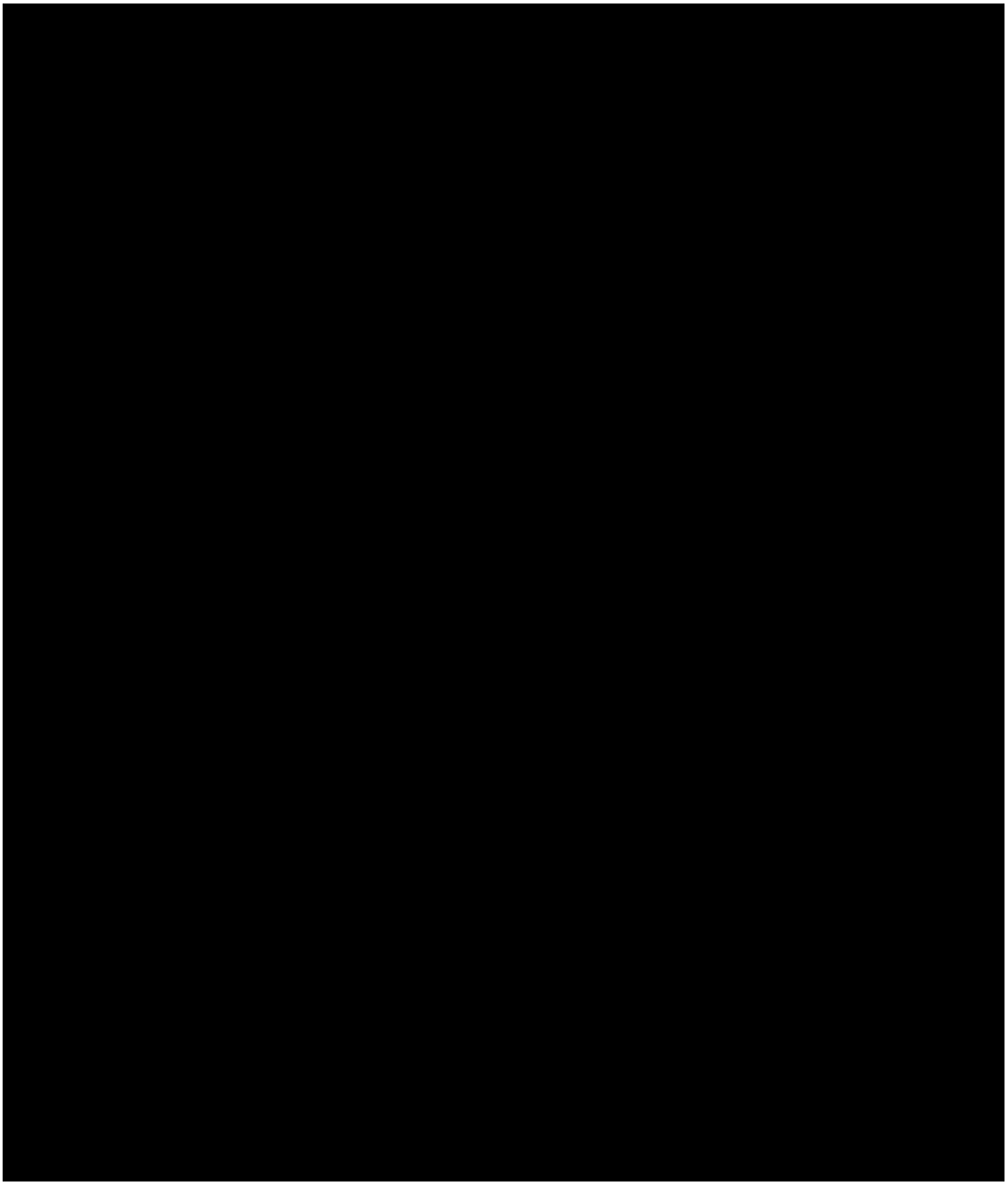

Figure 2.

Progressive cortical atrophy in *Ppt1*$^{-/-}$ mice. Cortical thickness measurements reveal progressive thinning of the cortical mantle that occurs at different rates between subfields that serve different functions. Compared with age matched controls (+/+), significant thinning of the cortical mantle in *Ppt1*$^{-/-}$ mice was first evident in the primary visual cortex (V1) at 5 months of age and was subsequently observed in the primary auditory cortex (Au1) and primary motor (M1) at 7 months of age (** $p<0.01$). A similar decline in the thickness of the somatosensory barrelfield (S1BF) cortex was also evident in *Ppt1*$^{-/-}$ mice, but did not reach statistical significance. In contrast, cortical atrophy in the entorhinal (LEnt) cortex was less pronounced in *Ppt1*$^{-/-}$ mice.

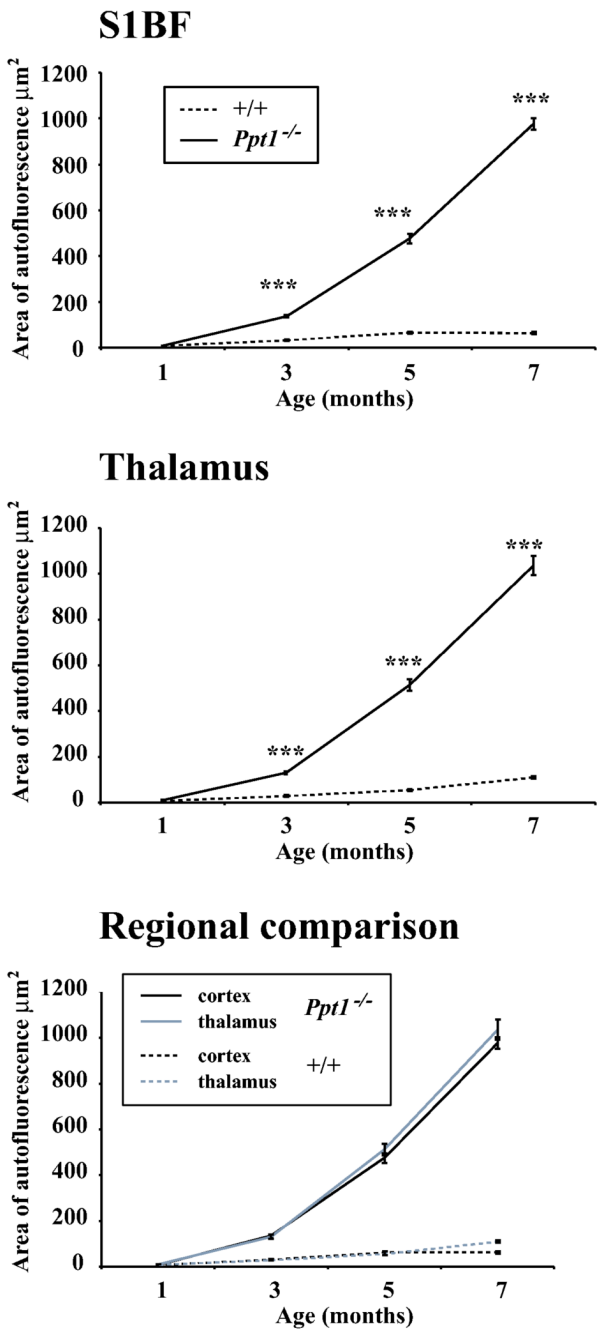

Figure 3.

Progressive accumulation of autofluorescent storage material in *Ppt1*$^{-/-}$ mice. Graphs of the relative amount of autofluorescent storage material over time reveal the progressive increase in storage material in the somatosensory barrelfield cortex (S1BF) and thalamus of *Ppt1*$^{-/-}$ mice compared with age-matched controls (+/+). Direct comparison of storage material accumulation revealed the similar rates of its accumulation in both regions.

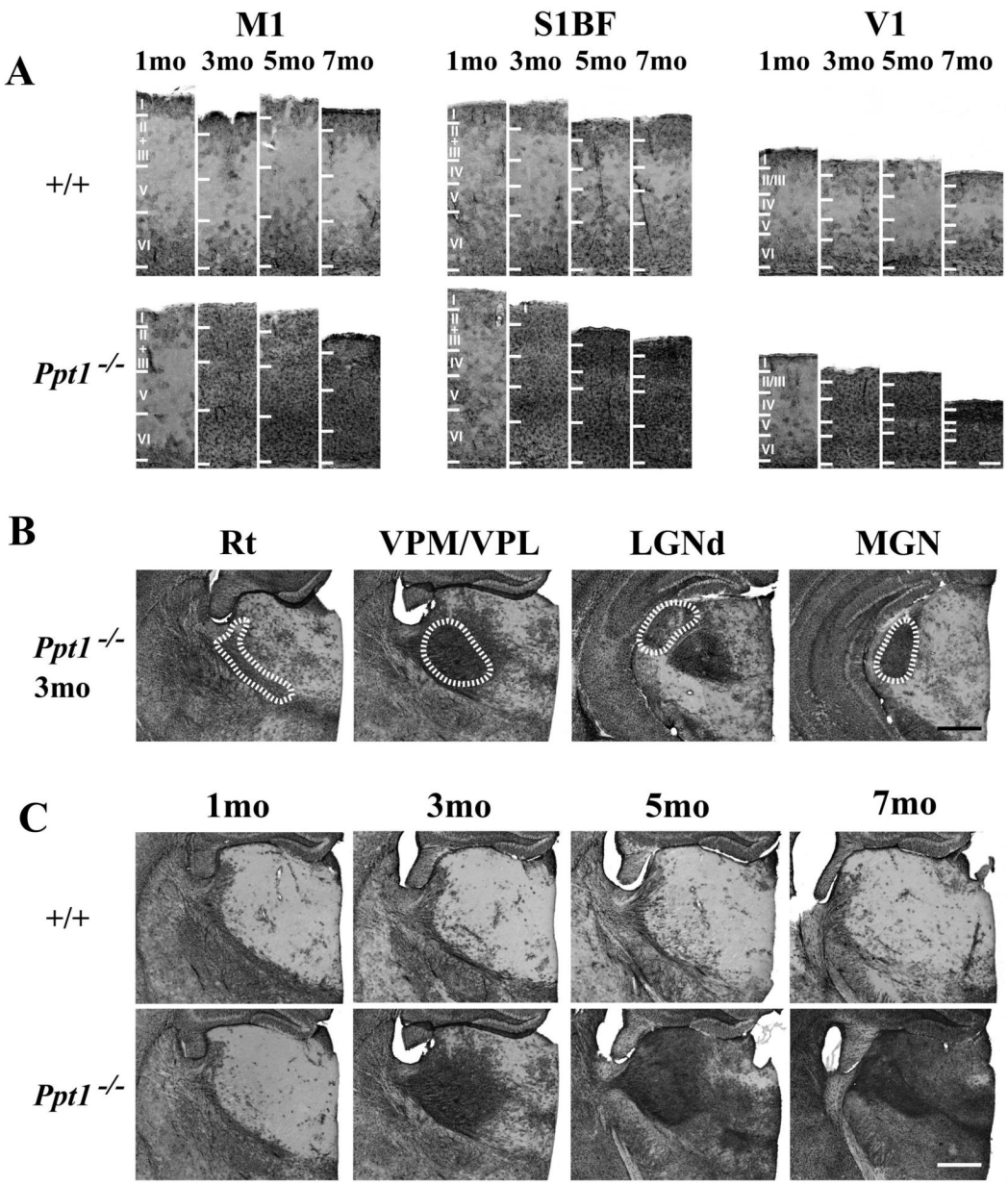

Figure 4.

Progressive astrocytosis in Ppt1$^{-/-}$ mice. (A) Immunohistochemical staining for glial fibrillary associated protein (GFAP) reveals the pronounced upregulation of this marker of astrocytosis with increased age in the primary motor cortex (M1), somatosensory barrelfield cortex (S1BF) and primary visual cortex (V1) of Ppt1$^{-/-}$ mice compared to age matched controls (+/+). GFAP immunoreactive astrocytes were evident within all laminae of M1, S1BF and V1 of mutant mice from 3 months of age onwards, initially most prominently in deeper laminae, but spreading to involve all laminae and increasing in intensity with disease progression. Laminar boundaries are indicated by roman numerals. (B) At 3 months of age Ppt1$^{-/-}$ mice exhibit pronounced astrocytosis that is confined to individual thalamic nuclei, with GFAP-positive

astrocytes prominent in the reticular (Rt), ventral posterior (VPM/VPL), lateral dorsal geniculate (LGNd) and medial geniculate (MGN) nuclei. The boundaries of these nuclei are indicated by white dashed lines. (C) Progressive accumulation of GFAP staining in the thalamus of $Ppt1^{-/-}$ mice compared to age matched controls at 1, 3, 5 and 7 months of age. Scale bar = 400 μm in A; 200 μm in B and C.

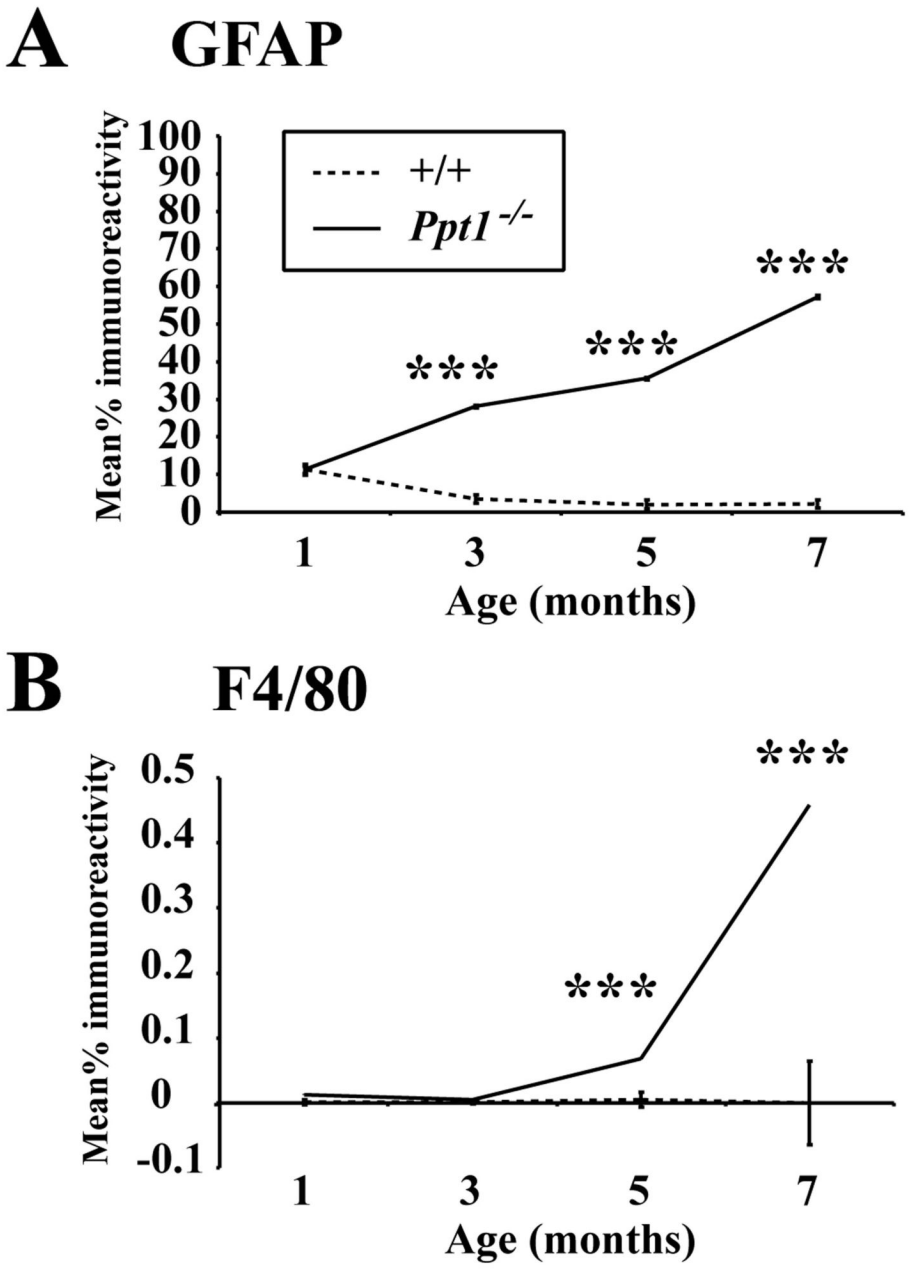

Figure 5.

Quantitative thresholding image analysis of GFAP (A) and F4/80 (B) immunoreactivity in the somatosensory barrelfield cortex (S1BF) demonstrates the progressive increase in these markers with disease progression in $Ppt1^{-/-}$ mice compared with age matched controls (+/+). (A) GFAP immunoreactivity was first significantly elevated in $Ppt1^{-/-}$ mice at 3 months of age and continued to increase during disease progression. (B) F4/80 immunoreactivity in $Ppt1^{-/-}$ mice was first significantly elevated in $Ppt1^{-/-}$ mice at 5 months of age and increased further at 7 months of age. (***, $p<0.001$, ANOVA with post-hoc Bonferroni analysis).

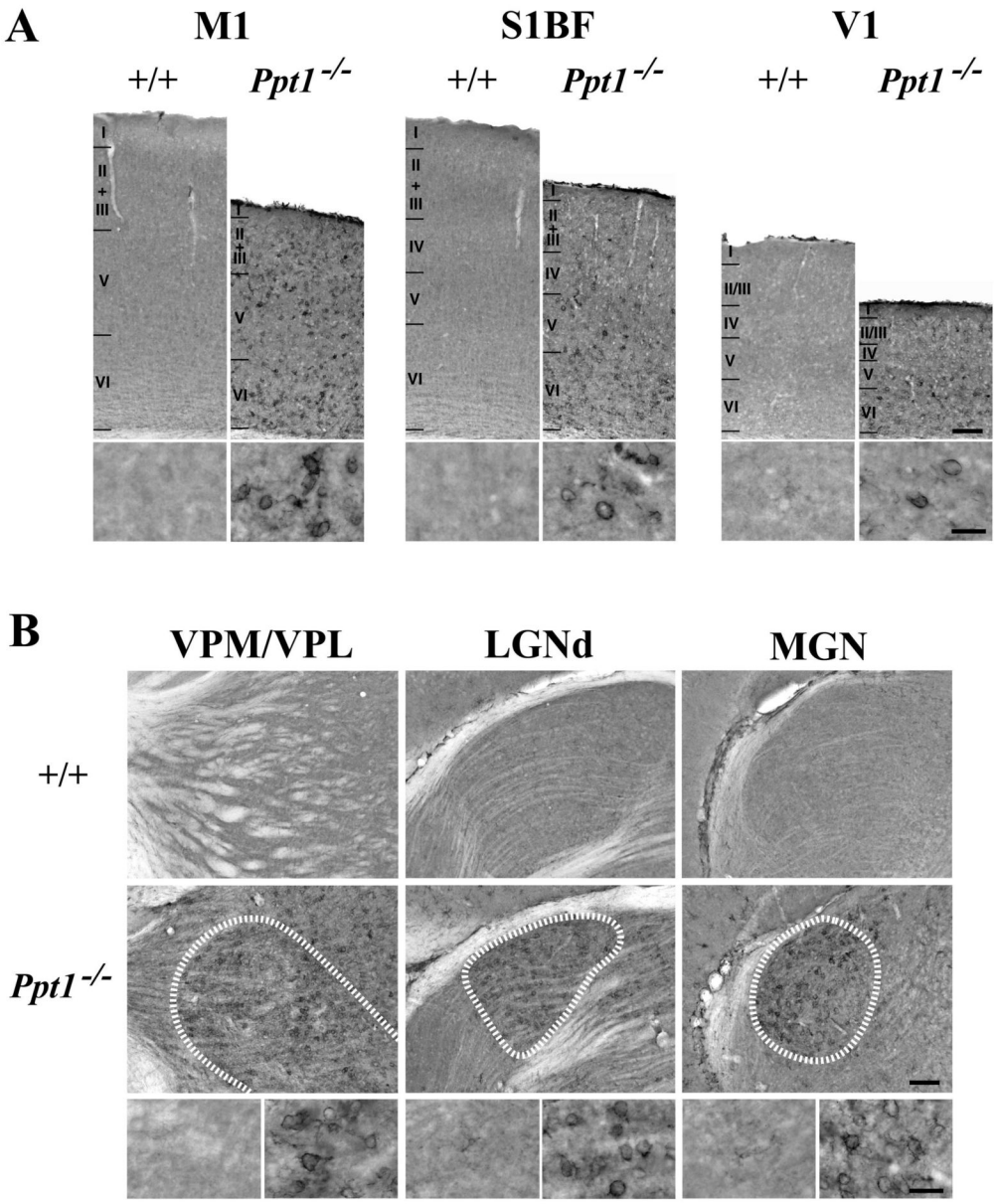

Figure 6.

(A) Activation of microglia in 7 month old Ppt1$^{-/-}$ mice. Immunohistochemical staining for the microglial marker F4/80 reveals activated microglia within all laminae of the primary motor cortex (M1), somatosensory cortex (S1BF) and primary visual cortex (V1) of Ppt1$^{-/-}$ mice at 7 months of age compared to age matched control mice (+/+). Many F4/80 immunoreactive microglia with swollen soma and retracted processes were present in mutant mice, but were absent in controls. Laminar boundaries are indicated by roman numerals. (B) Localized microglial activation within individual thalamic nuclei of 7 month old Ppt1$^{-/-}$ mice is also revealed by F4/80 immunoreactivity. In these mutant mice, intensely stained F4/80 positive microglia with brain macrophage like morphology were present in the ventral posterior (VPM/

VPL), dorsal lateral geniculate (LGNd) and medial geniculate (MGN) nuclei, but were virtually absent from adjacent thalamic nuclei and were not present in age matched controls. The boundaries of these nuclei are indicated by white dashed lines. Scale bar = 300 μm in A, B; 100 μm in inserts in A, B.

Figure 7.

Progressive loss of thalamic neurons in *Ppt1*$^{-/-}$ mice. Histograms of unbiased optical fractionator estimates of the number of Nissl stained thalamic relay neurons in the dorsal lateral geniculate nucleus (LGNd), medial geniculate nucleus (MGN), ventral posterior nucleus (VPM/VPL) and parvalbumin stained inhibitory neurons in the reticular thalamic nucleus (Rt PV) of *Ppt1*$^{-/-}$ mice and age-matched controls (+/+) at different stages of disease progression. The number of neurons in each of these thalamic nuclei declined in *Ppt1*$^{-/-}$ mice with increased age, but this occurred at different rates between nuclei. Neuron loss in mutant mice first became significant within the visual system (LGNd) at 3 months of age, but was relatively delayed in somatosensory (VPM/VPL) or auditory (MGN) relay nuclei and for inhibitory neurons (Rt). (* $p<0.05$; ** $p<0.01$; *** $p<0.001$, ANOVA with post-hoc Bonferroni analysis).

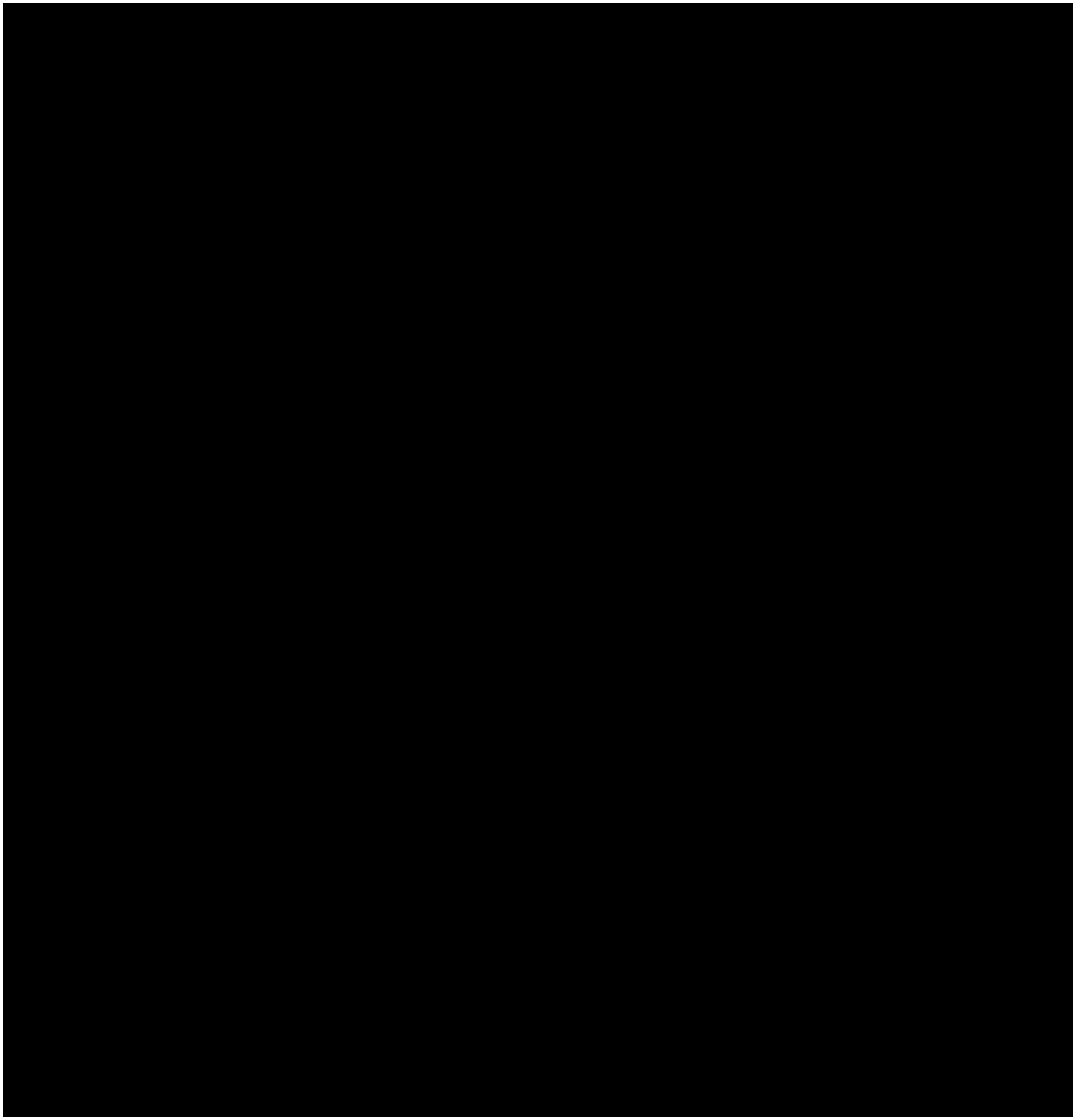

Figure 8.

Progressive loss of cortical neurons in *Ppt1*$^{-/-}$ mice. Histograms of unbiased optical fractionator estimates of the number of Nissl stained lamina IV granule neurons and somatostatin- (SOM) and parvalbumin- (PV) positive neurons in the primary visual (V1) and somatosensory barrelfield (S1BF) cortex of *Ppt1*$^{-/-}$ mice and age-matched controls (+/+) at different stages of disease progression. In V1 of mutant mice a significant loss of lamina IV granule neurons and SOM- or PV-positive interneurons was already evident at 5 months of age. SOM-positive interneurons were also significantly reduced in number at 5 months of age in S1BF of *Ppt1*$^{-/-}$ mice, but the significant loss of PV-positive interneurons and granule

neuron populations in S1BF did not occur until 7 months of age. (** $p<0.01$; *** $p<0.001$, ANOVA with post-hoc Bonferroni analysis).

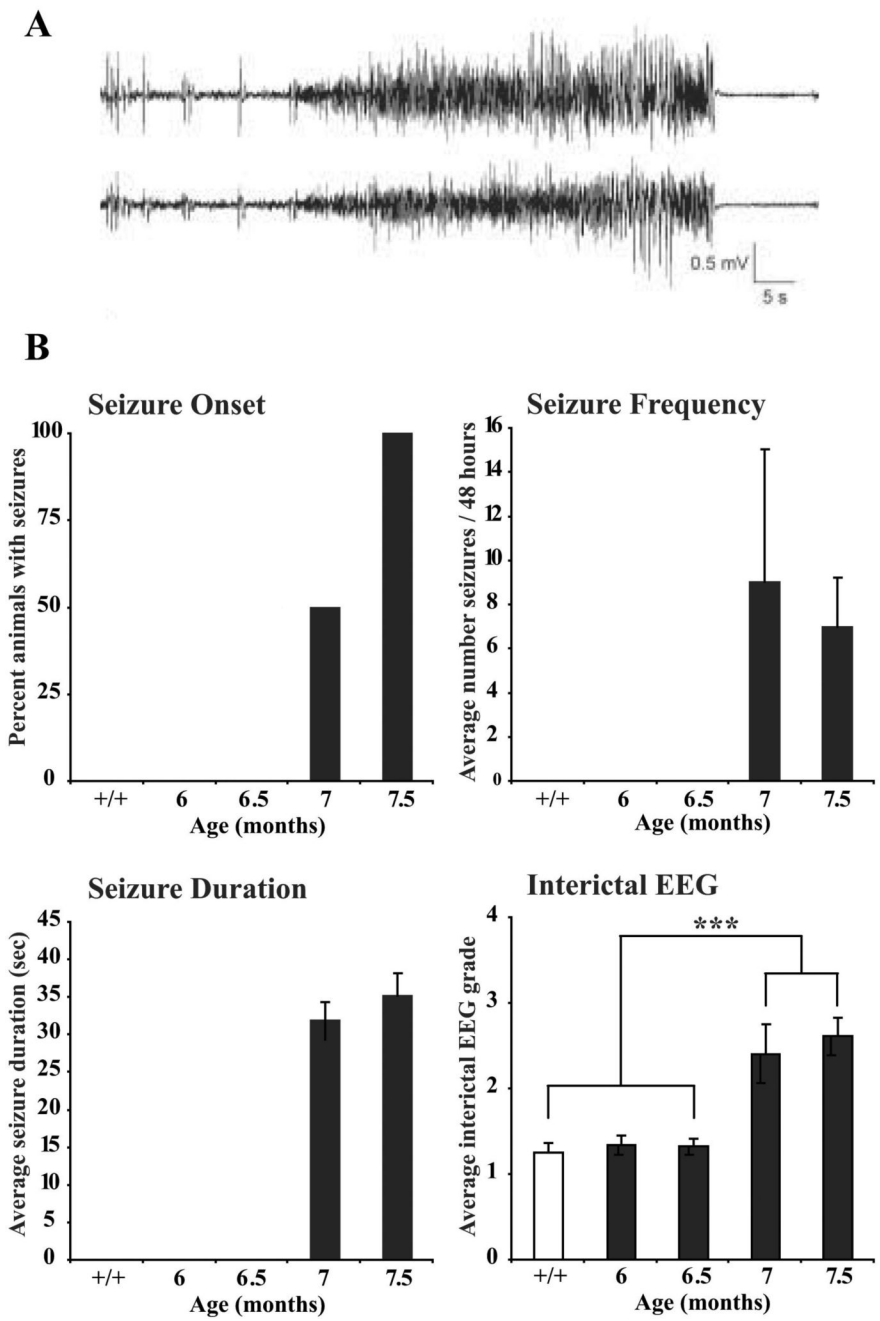

Figure 9.

Progressive development of the seizure phenotype of *Ppt1*$^{-/-}$ mice. (A, B) electroencephalogram (EEG) recordings made via chronically implanted epidural screw electrodes revealed the onset and nature of spontaneous seizure activity in *Ppt1*$^{-/-}$ mice with increased age. (A) Representative example of a seizure recorded in a Ppt1$^{-/-}$ mouse by two channel EEG. (B) Seizures were not evident in *Ppt1*$^{-/-}$ mice until 7 months of age and were present in all mutant mice by 7.5 months of age, but were not present in age matched controls (+/+). There was no significant difference between mutant mice in the frequency or duration of seizures at 7 and 7.5 months of age. Graded scoring of EEG recording traces also revealed a significant worsening of the interictal background EEG in mutant mice above 7 months of

age, compared to mutant mice at 6 and 6.5 months of age and age-matched controls. (*** $p<0.001$, ANOVA with post-hoc Tukey-Kramer multiple comparisons).